Original Research

M.J. Truex*
T.C. Johnson
C.E. Strickland
J.E. Peterson
S.S. Hubbard

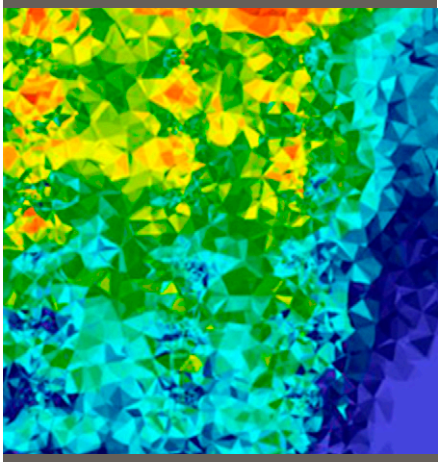

Neutron moisture logging, cross-hole electrical resistivity tomography, and cross-hole ground-penetrating radar approaches were evaluated with respect to their ability to provide effective spatial and temporal monitoring of moisture content changes during soil desiccation.

M.J. Truex, T.C. Johnson, and C.E. Strickland, Energy and Environment Directorate, Pacific Northwest National Lab, P.O. Box 999, MS K6-96, Richland, WA 99354; J.E. Peterson and S.S. Hubbard, Lawrence Berkeley National Lab., 1 Cyclotron Road, MS 90-1116, Berkeley, CA 94720. *Corresponding author (mj.truex@pnl.gov).

Vadose Zone J.
doi:10.2136/vzj2012.0147
Received 3 Oct. 2012.

© Soil Science Society of America
5585 Guilford Rd., Madison, WI 53711 USA.
All rights reserved. No part of this periodical may be reproduced or transmitted in any form or by any means, electronic or mechanical, including photocopying, recording, or any information storage and retrieval system, without permission in writing from the publisher.

Monitoring Vadose Zone Desiccation with Geophysical Methods

Soil desiccation was recently field tested as a potential vadose zone remediation technology. Desiccation removes water from the vadose zone and significantly decreases the aqueous-phase permeability of the desiccated zone, thereby decreasing movement of moisture and contaminants. The two- and three-dimensional distribution of moisture content reduction with time provides valuable information for desiccation operations and for determining when treatment goals have been reached. This type of information can be obtained through the use of geophysical methods. Neutron moisture logging, cross-hole electrical resistivity tomography, and cross-hole ground-penetrating radar approaches were evaluated with respect to their ability to provide effective spatial and temporal monitoring of desiccation during a treatability study conducted in the vadose zone of the USDOE Hanford site in the state of Washington.

Abbreviations: bgs, below ground surface; ERT, electrical resistivity tomography; GPR, ground-penetrating radar; VMC, volumetric moisture content.

In situ remediation is a potential approach to address contaminants located in the vadose zone at depths below the limit of direct exposure, where remediation is focused on protection of the groundwater (Dresel et al., 2011). Although a vast body of research has been performed to investigate in situ remediation of groundwater systems, significantly fewer studies have been dedicated to remediation of contaminated vadose zone regions. Concurrent with the development of remediation approaches, successful vadose zone remediation will also require effective methods of remedy performance monitoring. In 2008, the USDOE initiated a treatability test program to evaluate the potential of several deep vadose zone remedies for the protection of groundwater (USDOE, 2008), with assessment of approaches that mitigate the transport of inorganic and radionuclide contaminants from the vadose zone to the groundwater. Soil desiccation was investigated as a potential vadose zone remediation technology, including laboratory studies (Ward et al., 2008; Oostrom et al., 2009, 2012a, 2012b; Truex et al., 2011), modeling studies (Ward et al., 2008; Truex et al., 2011), and field testing (Truex et al., 2012a, 2012b) conducted as part of the treatability test efforts at the USDOE Hanford site.

Desiccation of a portion of the vadose zone, in conjunction with a surface infiltration barrier, has the potential for minimizing the migration of deep vadose zone contaminants toward the water table (Truex et al., 2011). To apply desiccation, a dry gas is injected into the subsurface. The dry gas evaporates water from the porous medium until the gas reaches 100% relative humidity and can no longer evaporate water. Evaporation can remove pore water and result in a very low moisture content in the desiccated zone (Ward et al., 2008; Oostrom et al., 2009; Truex et al., 2011). The desiccation process removes previously disposed and native water from the vadose zone and significantly decreases the water relative permeability of the desiccated zone. Due to these desiccation-induced changes, the future rate of movement of moisture and contaminants through this zone is decreased.

The performance of desiccation in terms of mitigating future moisture movement is related to the extent of moisture content reduction and the location and thickness of the desiccated zone (Truex et al., 2011, 2012a, 2012b). Reducing the moisture content below the residual moisture content value for the sediment is a target for desiccation because of the low resulting water relative permeability (Truex et al., 2012a, 2012b). Information about the distribution of the moisture content reduction with time is needed for performance monitoring during desiccation implementation. These data are important for determining when

desiccation has met treatment goals and thus when the process can be stopped. Monitoring data can also be used to guide operational decisions, such as adjustments in system flow rates and injection gas properties. While nominal values for these injection parameters can be selected based on initial site characterization data, the impact of subsurface heterogeneities cannot be fully predicted. As such, monitoring is needed to assess the impact of these heterogeneities on desiccation performance. The objective of this study was to evaluate the effectiveness of technologies for monitoring desiccation under field conditions. Several geophysical approaches were tested for monitoring desiccation-induced changes in moisture and temperature at the Hanford site desiccation field test, including neutron moisture logging, temperature logging, cross-hole ground-penetrating radar and cross-hole electrical resistivity tomography.

Geophysical methods have been used extensively in the last decade to characterize and monitor subsurface hydrologic processes (e.g., Rubin and Hubbard, 2005; Vereecken et al., 2006). Because geophysical data can be collected from many different platforms (e.g., from satellites and aircraft, at the ground surface of the Earth, and at or between wellbores), the geophysical data can provide remote subsurface characterization or monitoring information across a variety of spatial scales and resolutions. The main advantage of using geophysical data over conventional measurements is that geophysical methods can provide spatially extensive information about the subsurface in a minimally invasive manner at a comparatively high resolution. The greatest disadvantage is that the geophysical methods provide only indirect proxy information about subsurface hydrologic properties or processes.

Soil moisture content determination in the vicinity of a wellbore using neutron scattering probes has become a standard method in the past several decades (Hignett and Evett, 2002). A neutron probe consists of a high-energy neutron source, a low-energy or thermal neutron detector, and the electronics required for counting and storing the measured response. A fast neutron source manually placed within moist soil develops a dense cloud of thermal neutrons around it, and a thermal neutron detector placed near the source samples the density of the generated cloud. The concentration of thermalized neutrons is affected by both the soil density and its elemental composition. Elements that absorb neutrons are often in low concentration in the soil solid phase, and when the clay content is also low, the neutron probe response is mainly affected by changes in moisture content (Greacen et al., 1981; Hignett and Evett, 2002). Neutron moisture logging data can typically be collected with high vertical resolution and can be converted to volumetric moisture content (VMC) using published or site-specific relationships. Interpolation of neutron moisture logging data between multiple measurement wellbores can be used to generate an estimated two- or three-dimensional moisture content distribution.

Ground-penetrating radar (GPR) methods are also commonly used to characterize or monitor the subsurface moisture content. Ground-penetrating radar methods use electromagnetic energy at frequencies of ~10 MHz to 1GHz to probe the subsurface. At these frequencies, the dielectric polarization within a material that has been subjected to an external electric field dominates the electrical response. Ground-penetrating radar systems consist of an impulse generator that repeatedly sends a particular voltage and frequency signal to a transmitting antenna. Cross-hole GPR methods involve lowering a transmitter into a wellbore and measuring the vertical electrical field with a receiving antenna that is lowered down another wellbore. The transmitting and receiving antennas are manually relocated to different positions in the wellbores to facilitate transmission of the energy through a large fraction of the area between the measurement boreholes.

Together, the electrical properties of the host material and the frequency of the GPR signal primarily control the sampling volume and the depth of penetration of the signal. The electromagnetic velocity (V) is dependent on the permittivity (ε), conductivity (σ), frequency (ω), and magnetic permittivity (μ, assumed to be equal to free space) of the subsurface material through which the signal travels:

$$V = \left\{ \frac{\mu\varepsilon}{2} \left[\sqrt{1 + \left(\frac{\sigma}{\omega\varepsilon} \right)^2} + 1 \right] \right\}^{-1/2} \qquad [1]$$

The loss tangent is a useful metric for determining low-loss conditions and is defined as the electrical conductivity divided by the product of the dielectric permittivity and the angular frequency. In general, GPR performs better in low-loss environments, such as unsaturated coarse or moderately coarse textured soils. The GPR signal strength is strongly attenuated in electrically conductive environments (such as systems dominated by the presence of clays or high-ionic-strength pore fluids). When low-loss conditions prevail, the velocity depends primarily on the permittivity, which can be expressed as (Davis and Annan, 1989):

$$\varepsilon \approx \left(\frac{c}{V} \right)^2 \qquad [2]$$

where c is the propagation velocity of electromagnetic waves in free space. The velocity of the GPR signal can be obtained by measuring the travel time of the signal across a known distance between the transmitter and the receiver. Using measurements acquired from antennae located at many different vertical positions within each borehole and inversion algorithms, a two-dimensional image of GPR velocity between boreholes can be produced through tomographic inversion (e.g., Jackson and Tweeton, 1994; Peterson, 2001) and used with Eq. [2] to estimate the two-dimensional permittivity distribution.

Soil dielectric permittivity is strongly dependent on moisture content because of the large difference between the water and bulk soil permittivities. The relative permittivity (the dielectric permittivity of a material divided by the free-space permittivity, ε_0) of water is approximately 80, compared with values between 3 and 7 for typical soil mineral components. As such, under low-loss and unsaturated conditions, the GPR velocity is primarily influenced by the moisture variability and secondarily by texture, although texture can influence moisture dynamics and thus the effective GPR response (Grote et al., 2010). Studies have demonstrated that GPR methods can effectively estimate and monitor subsurface moisture content using measured electromagnetic velocities (Hubbard et al., 1997; Van Overmeeren et al., 1997; Huisman et al., 2001; Binley et al., 2002; Day-Lewis et al., 2002; Laloy et al., 2012). The dielectric permittivity of soils and sediments also depends on temperature (Or and Wraith, 1999). For this study, however, we considered temperature effects to be negligible based on laboratory core permittivity measurements made throughout the temperature range of this experiment, which corresponded to estimated VMC errors of <0.01 $m^3\ m^{-3}$ (data not shown).

Several different petrophysical relationships have been used to translate permittivity into moisture content estimates (Huisman et al., 2001). An example is shown in Eq. [3], where volumetric moisture content, θ, is a linear function of the square root of the soil apparent dielectric permittivity, ε_a (Ledieu et al., 1986; White and Zegelin, 1994; Topp and Ferré, 2002):

$$\theta = A\sqrt{\varepsilon_a} + B \qquad [3]$$

where A and B are fitted parameters. In this study, we used the coefficients determined by Topp and Reynolds (1998) of $A = 0.115$ and $B = -0.176$. The term *apparent* is used here to mean the dielectric permittivity value that is inferred from measurement of the velocity of an electromagnetic wave at a given frequency. In this study, water content values obtained using Eq. [3] deviated from those derived using the polynomial Topp's equation (Topp et al., 1980; Topp and Ferré, 2002) by <0.01 $m^3\ m^{-3}$. General guidelines for GPR acquisition, processing, and water content estimation have been provided by Annan (2005) and Huisman et al. (2001).

Electrical resistivity tomography (ERT) is a method of remotely imaging the electrical conductivity (C) of the subsurface that has been commonly used to monitor subsurface moisture variations (e.g., Binley and Kemna, 2005; Revil et al., 2012). For cross-hole ERT applications, electrodes installed within boreholes are used to strategically inject currents and measure the resulting potentials to produce a data set that is used to reconstruct the subsurface C structure (Daily and Owen, 1991; Johnson et al., 2010). In unsaturated sediments, C can be influenced by clay content, granulometric properties, salinity, and temperature (Lesmes and Friedman, 2005), although moisture content (Slater and Lesmes, 2002) often dominates the response. Thus, temporal changes in moisture content during desiccation can be monitored by imaging corresponding changes in C using ERT. General guidelines associated with ERT acquisition, inversion, and interpretation have been provided by Binley and Kemna (2005).

In granular materials with a nonconductive solid phase, the bulk C can be described according to (Revil et al., 2012)

$$C = \sigma_f \phi^m S_w^n + \phi^m S_w^{n-1} \beta_{(+)} \bar{Q}_V \qquad [4]$$

where σ_f is the fluid conductivity, ϕ is the porosity, S_w is the water saturation, m is the cementation exponent, n is the water saturation exponent, $\beta_{(+)}$ represents the mobility of the cations in the pore water, and $\bar{Q}_V$ is the charge per unit pore volume of the diffuse part of the electrical double layer. The first term of Eq. [4] describes the component of C arising from ionic current flow within the pore water (Archie, 1942). The second term of Eq. [4] describes the component of C arising from current flow along the pore–grain interface within the electrical double layer, the so-called surface conductivity. In clean, low-clay sands with relatively small surface area, C is dominated by the first term in Eq. [4]. The Hanford formation, where our experiment was conducted, is comprised of high-energy flood deposits, consisting of coarse gravels and sands with interbedded fine sands and silt-sized materials (Serne et al., 2009). We assumed, therefore, that the second term of Eq. [4] was insignificant and considered only the first term (e.g., Archie's law). Although we have no direct information supporting the validity of Archie's law, as demonstrated below, the comparison between changes in water content derived from C using Archie's law and the actual changes in water content measured by neutron probe are favorable, suggesting that our assumption is reasonable. In addition to the Archie's law assumption, the relationship between temporal changes in water saturation and the corresponding changes in C that occur during subsurface desiccation can be simplified under the following assumptions:

1. Porosity ϕ and cementation exponent m are constant with time. These parameters are dependent on the textural properties of the sediment, and this assumption may be appropriate for many sites.

2. Fluid conductivity σ_f is constant with time. This assumption is not strictly valid because ionic concentrations increase as pore water is evaporated during desiccation, but it may be appropriate for many sites. This assumption was validated with core-scale measurements in this case (data not shown) and also by comparison with neutron probe measurements of changes in water content.

3. Water saturation exponent n is independent of saturation. This assumption may be appropriate for many sites, although at low water saturation values (less than ~5%), n has been observed to decrease with decreasing water saturation (Waxman and Smits, 1968; Han et al., 2009; Hamamoto et al., 2010).

If the assumptions stated above are valid, a desiccation-induced change in water saturation can be derived from Eq. [4] in terms of the corresponding change in bulk C:

$$\frac{S_t}{S_0} = 10^{(1/n)\log_{10}(C_t/C_0)} \qquad [5]$$

where S_t is the water saturation at time t, S_0 is the predesiccation baseline water saturation, and C_t and C_0 are the corresponding bulk conductivities at time t and before desiccation. As we will show, errors arising from the assumptions leading to Eq. [5] exist but are not so large as to invalidate ERT-derived changes in saturation expressed through the saturation ratio. It is important to note that the same assumptions may not fare as well at other sites. Note also that the ratios of VMC and water saturation are equivalent. Because desiccation is a nonisothermal process, the effects of temperature on bulk conductivity must also be considered. The temperature dependence of bulk conductivity in the vadose zone is dependent on moisture content but is always monotonic (Waxman and Thomas, 1974).

Temperature sensors can also provide a means to monitor the progress and distribution of desiccation using a network of in situ sensors. Temperature decreases due to evaporative cooling until the desiccation front reaches the monitoring locations (i.e., the time when the sediment between the injection location and the monitoring location is desiccated). At that time, the temperature at the monitoring location begins to increase toward the temperature of the injected gas because evaporative cooling is no longer occurring in the sediment between the injection location and the monitoring location (Oostrom et al., 2009). There can be multiple inflection points if there are multiple layers that are being desiccated at different rates and these layers are within a region that can impact the temperature at the monitoring location.

This study assessed selected geophysical monitoring approaches applied before and during the desiccation field test at the Hanford site. The methods were evaluated with respect to their ability to provide effective spatial and temporal monitoring of desiccation. Benefits and limitations of the methods were considered based on the characteristics of the data collection and analysis techniques.

Geophysical Monitoring of Field Desiccation Experiment

Field Test Summary

The desiccation field test was conducted in the vadose zone at the USDOE Hanford site 200-BC-1 Operable Unit as described by Truex et al. (2012a, 2012b) and summarized below. The total thickness of the vadose zone beneath the 200-BC-1 Operable Unit is about 100 m. About 110 million L of aqueous waste containing high concentrations of solutes was disposed of at multiple engineered cribs and trenches, primarily in the 1950s. Figure 1 shows the predesiccation characterization data for vertical stratigraphy, electrical conductivity (corresponding to the contaminant distribution), and moisture distribution at the test site injection and extraction wells in relation to the well screen interval. The test was conducted within the Hanford formation and porous media

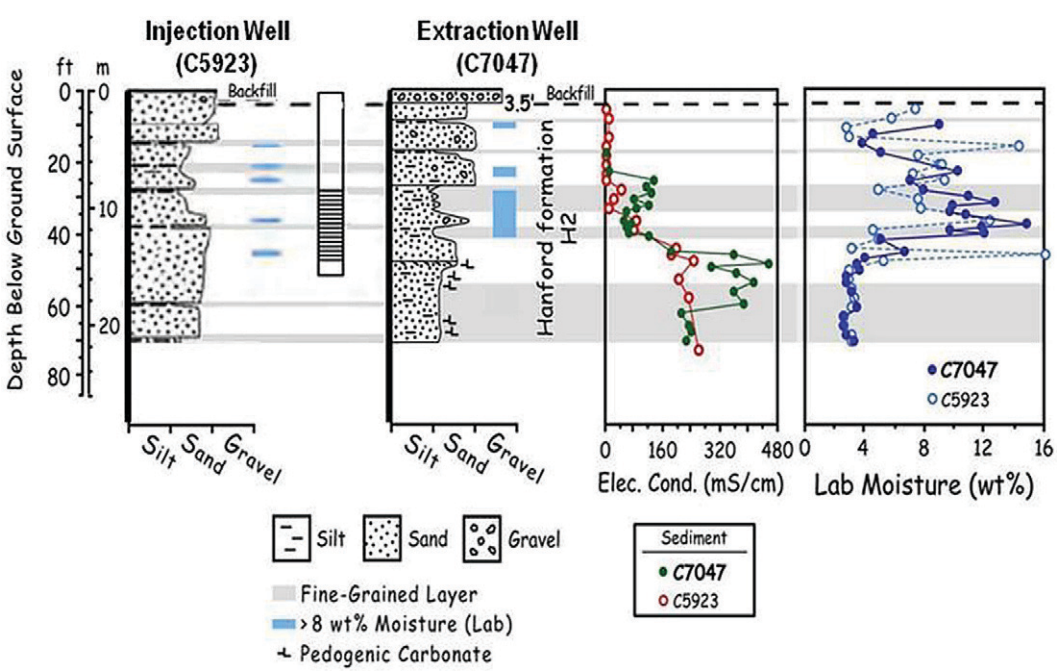

Fig. 1. Injection and extraction well borehole laboratory moisture content, extracted pore water electrical conductivity, and well screened interval (after USDOE, 2010; Serne et al., 2009; Um et al., 2009). Electrical conductivity was measured on pore water extracted from sediment samples.

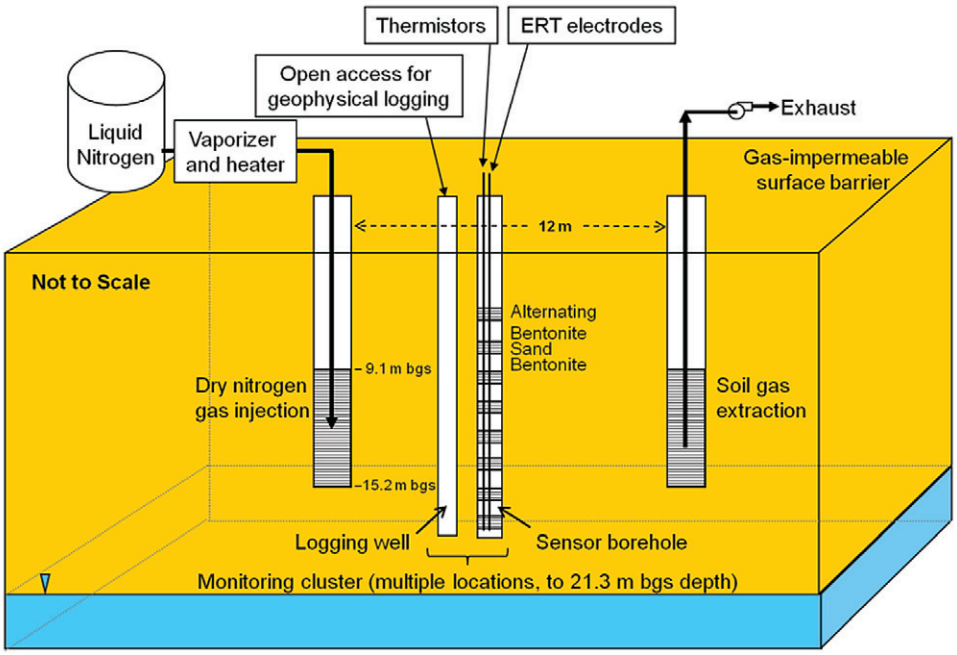

Fig. 2. Basic components of the desiccation field test system (ERT, electrical resistivity tomography; bgs, below ground surface).

grain-size variations in the test interval ranged from sand to loamy sand (which is similar to the porous media observed throughout the full depth interval). The injection well was located between adjacent waste disposal cribs where the subsurface was impacted by lateral movement of crib discharges.

A dipole configuration was used for the field test with injection of dry N_2 gas and extraction of soil gas through wells screened in a target depth interval from 9.1 to 15.2 m below ground surface (bgs) to favor soil gas flow within this interval and within a defined monitoring zone. The general operational and in situ monitoring strategy is depicted in Fig. 2. Use of dry N_2 gas at a controlled temperature of 20°C provided a constant inlet condition with a relative humidity of zero. Injection occurred at a stable flow rate of 510 $m^3\ h^{-1}$ from 17 Jan. through 30 June 2011 (164 d) except during a 13-d interval from 21 April through 4 May when there was no injection. Extraction of soil gas was maintained for the full test duration at a stable flow rate of 170 $m^3\ h^{-1}$. The injection and extraction wells were 12 m apart. Figure 3 depicts the lateral layout of injection and extraction wells and the monitoring locations. A 30- by 45-m gas-impermeable membrane barrier was installed at the surface centered over the well network to inhibit soil gas flow at the ground surface.

A clustered monitoring approach was used in the test whereby a sensor borehole, containing sensors for temperature and ERT electrodes, was placed nominally adjacent to a cased, unscreened logging well used to conduct manual neutron moisture logging and to acquire cross-hole GPR data. Sensor boreholes (21.3 m total depth)

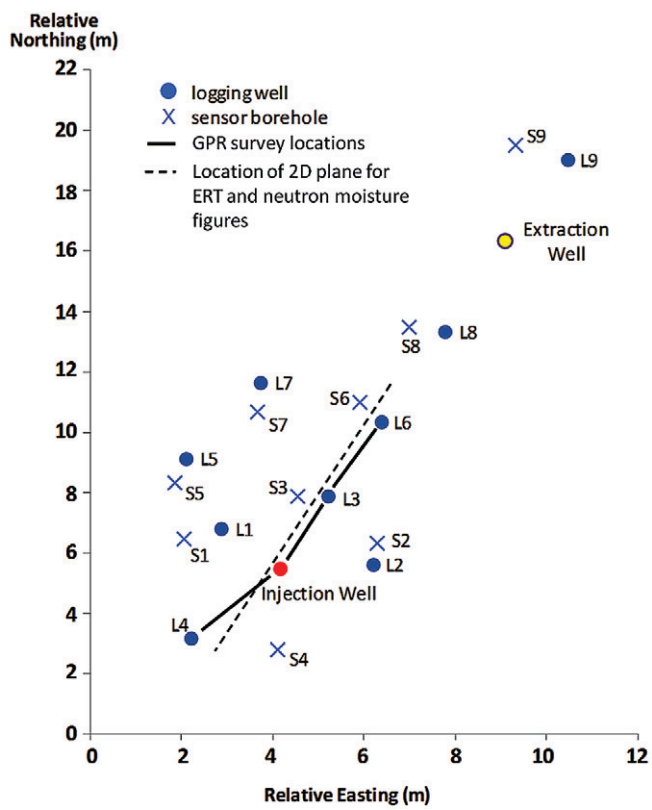

Fig. 3. Location of test site wells, where boreholes with an "S" designation contained in situ thermistors and electrical resistivity tomography (ERT) electrodes and wells with an "L" designation were cased wells for neutron logging and ground-penetrating radar (GPR) access (2D, two dimensional).

were constructed with alternating 0.76-m-thick zones of 100-mesh (>0.125- and <0.149-mm) Colorado sand (Colorado Silica) and granular bentonite from 3 to 21.3 m bgs. Electrical resistivity tomography electrodes were placed within the bentonite zones (e.g., every 1.5 m) with tubing installed to enable the addition of water around each electrode to locally hydrate the bentonite and maintain effective coupling between the electrode and the subsurface. Electrical connectivity was checked periodically during the test, and water was added when necessary to improve electrical coupling, where a threshold of >10 mA injected current was used to indicate suitable electrode coupling. Sensor boreholes also contained thermistors every 0.6 m from 3 to 21.3 m bgs. Logging wells extended to 21.3 m bgs with a 5.08-cm polyvinyl chloride casing (plugged at the bottom) in a 10.16-cm-diameter borehole and 100-mesh Colorado sand in the annular space.

Neutron Moisture Logging

Neutron moisture logging was conducted using a CPN 503DR Hydroprobe (InstroTek Inc.). Neutron probe measurements were acquired at depth increments of approximately 7.5 cm using a count time of 30 s and then converted to a count ratio (C_R) by dividing each measurement by the standard count.

Neutron probe data were converted to VMC using a site-specific relationship described by Truex et al. (2012a) and summarized below. Sediment samples were collected laterally within 0.9 m of the neutron logging well L2 (6–18 m bgs) after the active desiccation phase of the test, and the sediment texture ranged from medium sand to loamy sand with the exception of one sample of sandy silt. Although clay content can also affect moisture content calibration (Greacen et al., 1981), the clay content was low at the desiccation field site, ranging between 2.4 and 8%.

Samples were grouped into sand and loamy sand texture materials. Neutron moisture probe C_R data were plotted with corresponding post-desiccation laboratory-measured VMC (computed using measured gravimetric moisture content and bulk density) from samples at the same depth. Using only samples >0.05 $m^3\ m^{-3}$, a linear calibration relationship was observed for both sand and loamy sand. Post-desiccation VMC for some of the very dry core samples within the highly desiccated zones (loamy sand and sand textures) were $0.004 \pm 0.002\ m^3\ m^{-3}$ from laboratory gravimetric analyses, with corresponding C_R values of 0.21 ± 0.007. For the loamy sand, using the linear relationship based on only samples >0.05 $m^3\ m^{-3}$ would predict a C_R of 0.34 for a moisture content of 0.004 $m^3\ m^{-3}$, substantially different from the actual observations. Linear relationships across the full range of data could be applied but provide a poor fit to the data. For this study, a nonlinear neutron probe calibration relationship captured the response for both soil types and provided a better fit to the data across the full range (Fig. 4). Regression of the VMC (θ) and C_R data for all core samples resulted in the relationship $\theta = 0.714C_R^2 - 0.1363C_R$, with a root mean square error of 0.015 for θ and a coefficient of determination of 0.93.

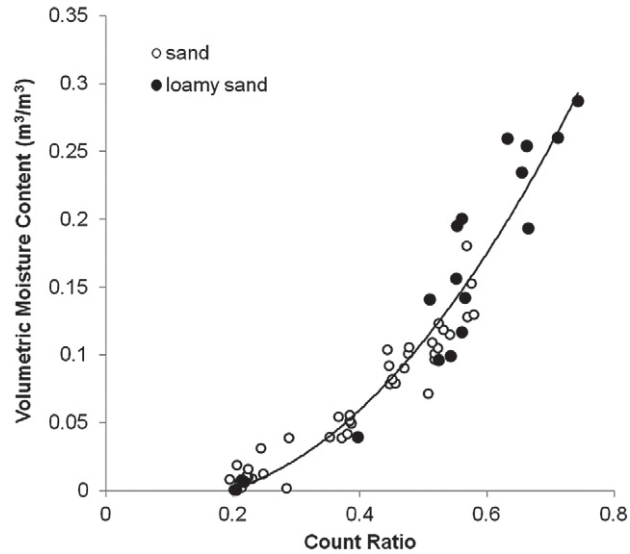

Fig. 4. Calibration relation for neutron moisture probe count ratio data and corresponding laboratory-measured volumetric moisture content (after Truex et al., 2012a).

Volumetric moisture content values from predesiccation and post-desiccation neutron logging events were interpolated to a finely spaced grid encompassing the logging wells using a weighted inverse-distance interpolation scheme. Due to the high vertical resolution of the data along the logging wells, the corresponding low lateral resolution, and the expected high lateral correlation in moisture content, we chose a 5:1 horizontal/vertical weighting in the interpolation. This interpolation provided a smoothed, three-dimensional estimate of VMC distribution.

Ground Penetrating Radar

Ground-penetrating radar data were collected with a PulseEKKO 100 using 100-MHz borehole antennas (Sensors and Software, Inc.). Multiple offset gather surveys (Peterson, 2001) were periodically collected between logging well pairs using a vertical offset increment of 0.25 m and an angular coverage of approximately 40° above and below the midpoint of each gather. Wellbore deviation logs were applied to more accurately determine the antenna positions used in the surveys. Borehole pair separation was roughly 3 m, and the primary transect was along the plane between the injection and extraction wells (Fig. 3). The first arrival times of the energy were picked from the data and were inverted using MIGRATOM, a curved-ray inversion software (Jackson and Tweeton, 1994), to yield two-dimensional electromagnetic velocity estimates along key transects. The data were inverted with no vertical-to-horizontal anisotropy and using global minimum and maximum velocity constraints of 0 and 0.25 m ns^{-1}, respectively. The results from each of the inversions produced travel time residual errors <1.9 ns. The velocity estimates were converted to dielectric permittivity using Eq. [2] (i.e., by assuming low-loss conditions). Equation [3] was used to convert GPR-derived permittivity to VMC content.

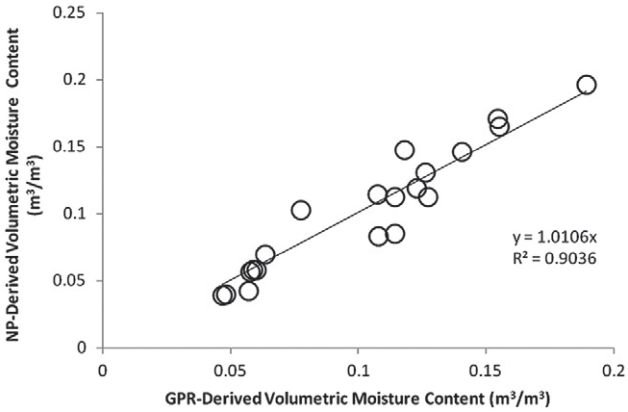

Fig. 5. Comparison of volumetric moisture content derived from ground-penetrating radar (GPR) and neutron moisture logging (NP) for Location L4 at depths <10 m before desiccation.

At the desiccation site, the C ranged up to 0.330 S m^{-1} and the low-loss assumption underlying Eq. [2] was not valid at all locations. Low-loss conditions are valid when the loss tangent is <<1. For instance, assuming a dielectric permittivity of 10 and a frequency of 100 MHz, the loss tangent will be <1 for C values <0.05 S m^{-1}. Before desiccation, ERT-derived C values were <0.05 S m^{-1} at depths <10 m. A comparison of baseline near-borehole VMC estimates from GPR (derived using Eq. [2] and [3]) to those obtained from neutron moisture logging indicated a good correlation for depths <10 m where C was <0.05 S m^{-1}. This comparison is shown in Fig. 5 for Borehole L3 and was similar for the other boreholes at the desiccation test site. At depths >10 m, the C value was higher than the low-loss assumption cutoff, and the linear relationship between VMC estimated from neutron moisture logging and GPR was degraded. Interpretation of GPR data for conditions with higher conductivity will be impacted by violation of the low-loss assumption, which can change during the desiccation process, as discussed below.

Electrical Resistivity Tomography

Electrical resistivity tomography data were collected before and during desiccation using 99 electrodes—11 electrodes equally spaced from 6.25 to 21.5 m deep in each of the nine sensor wells. Measurements were collected using an eight-channel MPT DAS-1 impedance tomography system (Multiphase Technologies, LLC). Full forward and reciprocal measurements were collected twice per day to estimate data noise and quality; each data set contained 6114 measurements after filtering. The data were collected and inverted in three dimensions with isotropic (i.e., equal weighting in all directions), first-order, spatial derivative smoothing constraints on an unstructured tetrahedral mesh with 354,544 elements. The parallel ERT inversion software described by Johnson et al. (2010) was used to invert each data set using 100 processors on parallel computing resources housed at the Pacific Northwest National Laboratory. Elements were refined around electrodes and within the imaging region to optimize simulation accuracy and available resolution. Each data set was individually inverted (i.e., no constraints were applied in the time dimension), and Eq. [5] was used to compute the saturation ratio for each element at each ERT survey time.

Core-scale testing on site sediments showed the C response to be primarily governed by decreases in water saturation as opposed to increases in fluid conductivity during desiccation, validating the assumption that fluid conductivity (σ_f) may be considered constant in time (data not shown). In addition, laboratory testing on site sediments showed n to be ~2.0 within the saturation range indicated by neutron moisture logging data during the desiccation test, and a constant value of 2.0 was used in Eq. [5]. The ERT images were also corrected for temperature before applying Eq. [5]. Laboratory testing on Hanford site sediments showed a temperature dependence of 0.00017 S m^{-1} °C^{-1} at 5% VMC and 0.00023 S m^{-1} °C^{-1} at 12% VMC, consistent with published values (Friedman, 2005; Ma et al., 2011). A constant value of 0.00020 S m^{-1} °C^{-1} was assumed for the temperature dependence and used to correct all C results to a temperature of 20°C based on the interpolated temperature field.

In order for a sequence of time-lapse ERT inversions to be comparable, each inverted data set must contain the same survey configuration and the same number of measurements. This requirement is problematic when data quality degrades during the course of the monitoring period. At the desiccation site, electrodes were installed within a plug of bentonite to facilitate electrical coupling with the host material. Some electrodes within the desiccation zone became poorly coupled to the host material on drying, probably due to bentonite shrinkage and cracking. Measurements using these electrodes had to be removed from every survey in the entire data set to produce a consistent set of measurements for the time-lapse inversion. This resulted in a loss of sensitivity and image resolution at depth. Figure 6 shows the squared sensitivity of the ERT measurements to the bulk conductivity distribution predesiccation (left) and post-desiccation (right) along a two-dimensional transect intersecting the injection and extraction wells. The post-desiccation decrease in sensitivity in the lower section and below the injection well was caused by the loss of electrodes during desiccation, resulting in an inability to resolve changes below about the 15-m depth. This is important when interpreting the time-lapse inversion images, which do not indicate the decreases in conductivity below 15 m that were indicated by neutron logging and radar. Note that this problem can be addressed in future applications by encasing the electrodes in a material less prone to desiccation cracking such as Portland cement grout.

Temperature Monitoring

Thermistors (USP8242 encapsulated negative temperature coefficient thermistors, U.S. Sensor) were used to monitor temperature. To achieve accurate temperature measurements across the range of interest, a fifth-order polynomial was used to relate resistance to temperature for each of the thermistors used in the field test. The manufacturer's calibration relationship was verified for a subset of

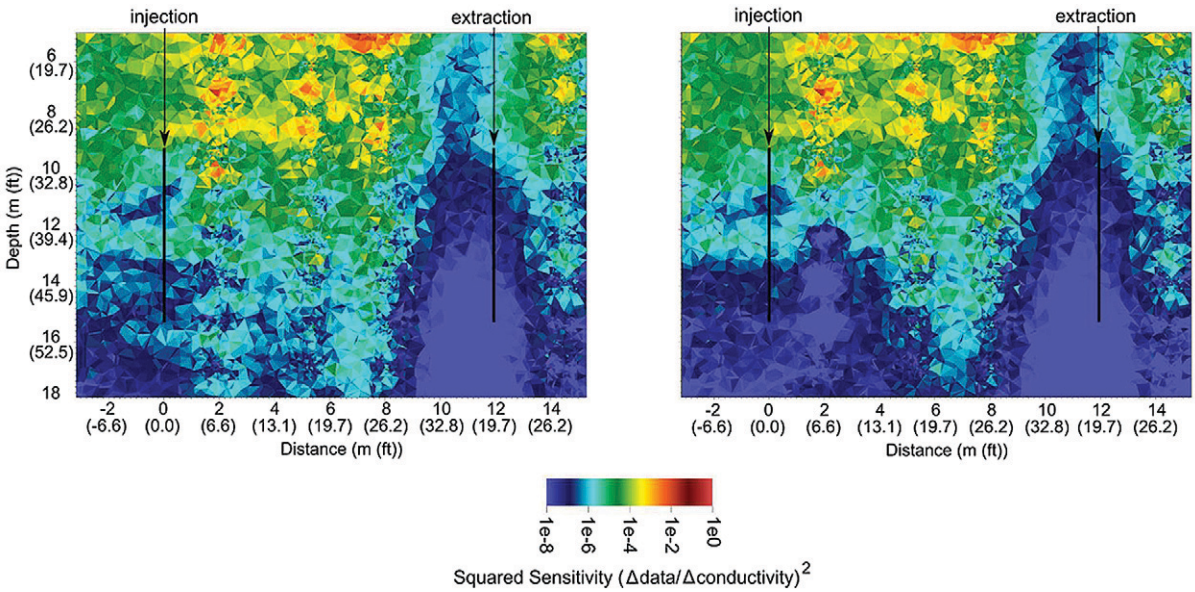

Fig. 6. Electrical resistivity tomography data sensitivity distribution for given data available before desiccation (left) and after desiccation (right). The loss in sensitivity surrounding the injection well from approximately the 14- to 16-m depth is caused by a loss of electrode coupling within the desiccation zone. The images are shown in true dimension (i.e., no smoothing between tetrahedral elements was applied).

the thermistors in a precision water bath spanning the 0 to 40°C temperature range, with measured accuracies >0.07°C.

Temperatures were logged continuously (10-min intervals) at each thermistor. In addition to use for correcting the ERT-derived *C* values to a standard temperature before using the ERT data for estimating VMC changes, three-dimensional interpolation of the temperature data was also used to evaluate the desiccation progress. The three-dimensional temperature field was estimated at selected times using the same interpolation technique that was used for the neutron moisture data.

Results and Discussion

Neutron moisture logging provides a large number of vertically discrete data points at multiple lateral locations with time. These data are expected to provide the most accurate and high-resolution information about vertical variations in moisture at the borehole locations. Cross-hole ERT and cross-hole GPR are expected to provide indirect but more spatially extensive estimates of moisture content and associated changes with time. The ERT data were collected autonomously over several boreholes and thus offer temporally dense information in three dimensions; the GPR data were collected manually and offer high two-dimensional spatial resolution but low temporal resolution. The temperature sensors provided a large number of vertically discrete data points at multiple lateral locations across the test zone and for multiple time points. We now describe the data sets and their associated interpretations in terms of monitoring the distribution of moisture content reduction with time to at or below a specified threshold moisture content value. We compare the different data suites and discuss their relative benefits and limitations for monitoring a desiccation treatment zone.

Field Test Data

Neutron moisture logging data with time show changes in the VMC at monitored locations that varied with depth and the initial moisture content associated with the sediment texture (e.g., Fig. 7). Neutron logging data are expected to be an accurate localized indicator of VMC because of their calibration to physical measurements of moisture content from sediment samples. Desiccation was not uniform across the injection screen depth interval. At each monitoring location, the neutron data show the vertical distribution of desiccation, and zones desiccated to below selected threshold moisture content values can be identified. For instance at Location L2, the depth interval between about 13 and 17 m bgs was desiccated to a VMC <0.02 $m^3\ m^{-3}$ by the end of active desiccation. The three-dimensional distribution of desiccation can be estimated by interpolating the neutron moisture logging data between monitoring locations. Figure 8 shows the VMC for a two-dimensional plane within the three-dimensional neutron moisture data interpolation. The distribution of moisture content with time can be used to identify where desiccation has reached a specified threshold moisture content, nominally in the 13- to 17-m depth interval out to a radial distance of about 3 m from the injection well for a moisture content threshold of 0.02 $m^3\ m^{-3}$ (red zone) by the end of active desiccation in the field test. Interpretation of the two-dimensional moisture content representation should consider that interpolation does not incorporate subsurface conditions that can impact the distribution of desiccation away from the measurement point.

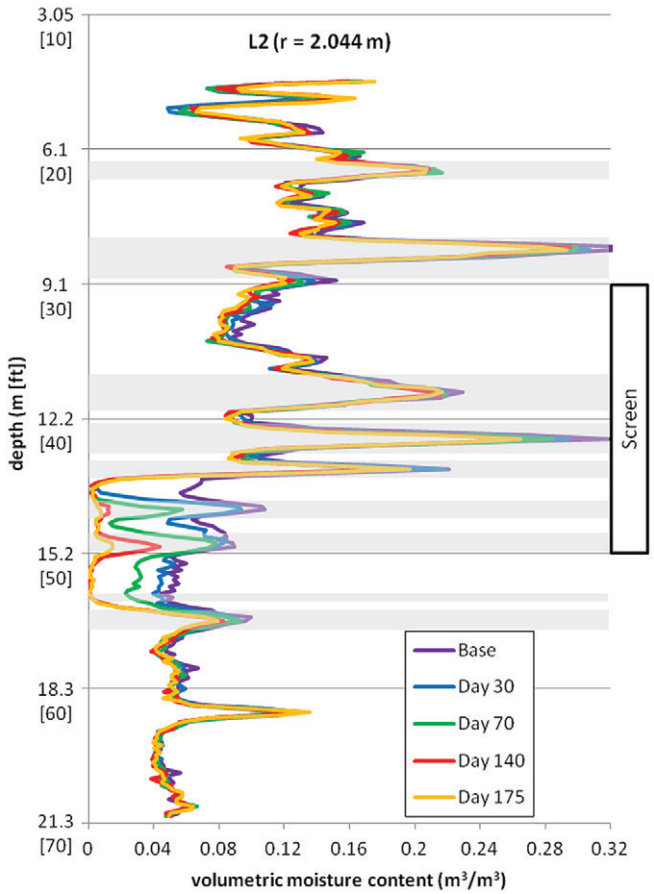

Fig. 7. Neutron moisture data at Location L2 in days from the start of active desiccation. Base data are predesiccation. Day 175 represents the end of active desiccation. Zones of loamy sand (gray) and sand (no shading) textures are shown for the depth interval 6 to 18 m below ground surface, where samples were evaluated from a post-desiccation borehole located 0.9 m away (adapted from Truex et al., 2012a).

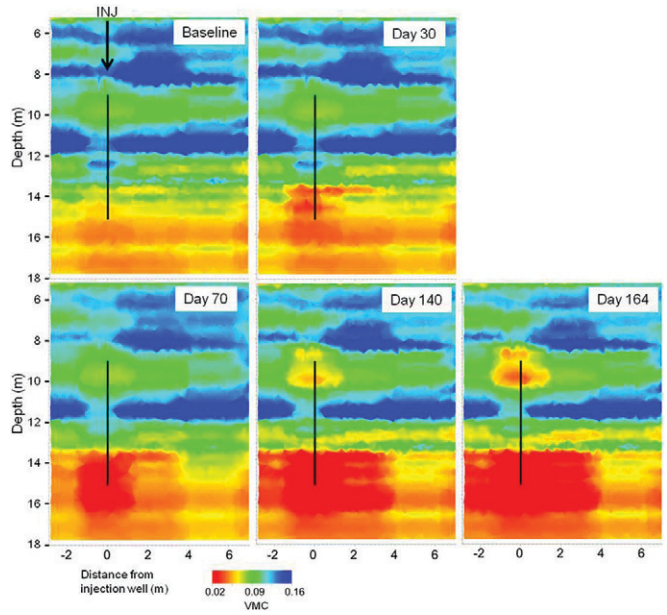

Fig. 8. Interpolation of volumetric moisture content (VMC) from neutron moisture logging data along the axis between the injection (INJ) and extraction wells. Neutron moisture data are from logging at Locations L1 to L7 (Fig. 3). The black line indicates the screened section of the injection well.

The two-dimensional distribution of desiccation between access wells can also be estimated by cross-hole GPR. Figure 9 shows the VMC with time for a series of two-dimensional GPR surveys between adjacent logging wells (Fig. 3). This figure was created using Eq. [2] and [3], recognizing that the validity of the low-loss assumption associated with Eq. [2] varies both spatially and temporally. Similar to the neutron moisture data, this estimate for the distribution of moisture content with time shows desiccation in the 13- to 17-m depth interval out to a radial distance of about 3 m from the injection well for a moisture content threshold of 0.02 $m^3\ m^{-3}$ (dark red zone) by the end of active desiccation in the field test. Interpretation of the two-dimensional moisture content representation should consider that conversion of GPR-derived permittivity to VMC is impacted by the C. Desiccation reduces the C, however, which renders GPR data acquisition more favorable and improves the accuracy of the GPR-derived moisture content estimate. For example, Fig. 10 shows the ERT-derived C distribution along the GPR survey transect before the start of the test (left) and at Day 140 of desiccation (right). The black regions

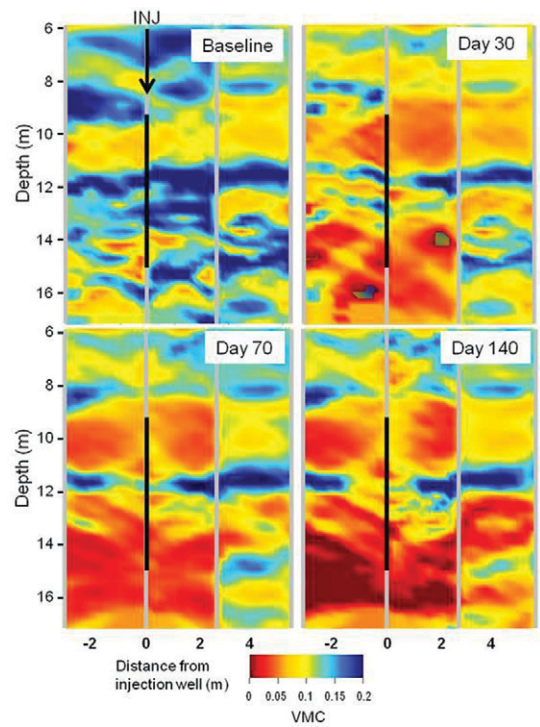

Fig. 9. Two-dimensional interpretation of volumetric moisture content (VMC) from cross-hole ground-penetrating radar data. Locations where the low-loss assumption is valid also need to be considered for interpretation of the VMC. Gray vertical lines are the locations of the logging wells. The black line indicates the screened section of the injection well.

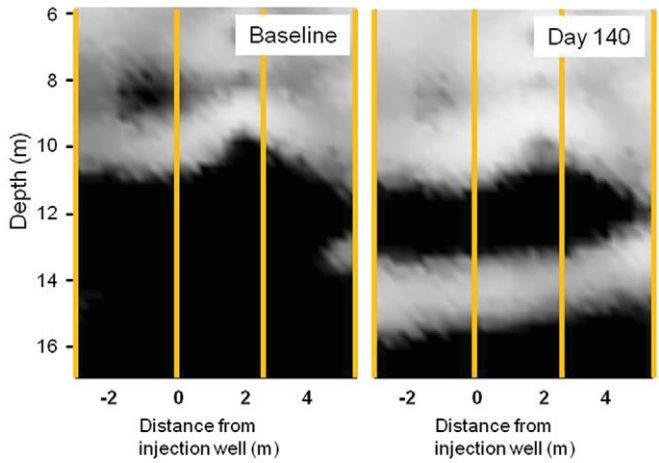

Fig. 10. Electrical conductivity distribution showing regions where the low-loss conditions can be assumed (light regions). Black regions show where the electrical conductivity is >0.05 S m^{-1} and the low-loss assumption cannot be applied. Yellow vertical lines are the locations of the logging wells.

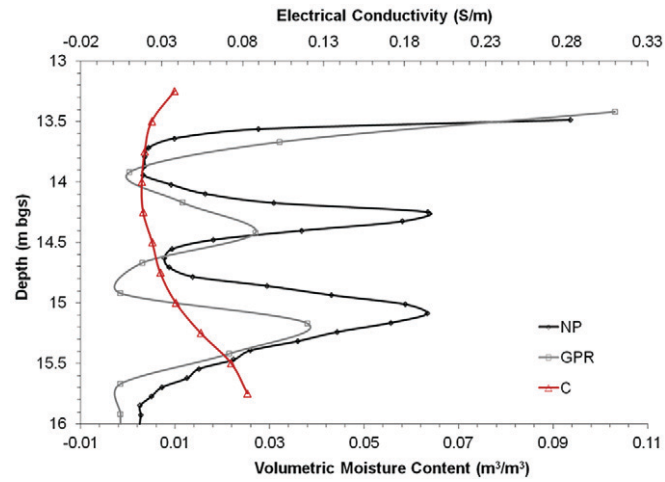

Fig. 11. Comparison of post-desiccation volumetric moisture content from ground-penetrating radar (GPR) and neutron moisture logging (NP) for Location L3 within a depth interval (bgs, below ground surface) where electrical conductivity (*C*) has been decreased by desiccation (light regions in Fig. 10).

illustrate where low-loss assumptions may not be valid ($C > 0.05$ S m^{-1}). Before desiccation, the low-loss assumption was generally valid above a depth of 10 m and invalid below 10 m. At the end of desiccation, low-conductivity conditions had been established within a zone from approximately the 13- to 15-m depth. Within this depth interval, GPR-derived moisture content estimates correlate well with estimates from neutron moisture logging (Fig. 11). Thus, within zones where desiccation has decreased the *C*, GPR can be used with confidence to estimate the moisture content distribution between wells. At other locations, the estimates should be considered with caution.

The progression and distribution of moisture content changes as imaged by ERT is shown in Fig. 12. The ERT data show changes in the VMC expressed as the ratio of the VMC at the time of measurement (VMC_t) to the baseline VMC from an ERT data set collected before desiccation (VMC_0), estimated as described in Eq. [5] and with recognition that the ratios of VMC and water saturation are equivalent. Thus, $VMC_t/VMC_0 = 1$ designates areas that have not changed from the conditions before active desiccation. Ratios <1 indicate desiccation, for instance, where a ratio of 0.5 means that the VMC is 0.5 times what it was before desiccation. The representations shown in Fig. 12 are for a two-dimensional plane extracted from three-dimensional ERT images. Areas where the VMC_t/VMC_0 ratio becomes less than a specified value (e.g., 0.5) could be used to interpret the distribution of desiccation below a threshold of change (moisture content decreased by half) or below an absolute threshold if used in conjunction with knowledge of the starting moisture content. The resolution of the ERT data inversion is on the order of 1 m^3. Thus, the ERT images in Fig. 12 do not resolve sharp contrasts in drying zones with time but show a "smoothed" image of how the subsurface is changing. Note that changes below approximately 15 m were not resolved by the ERT due to electrode loss as discussed above.

Figure 13 shows the temperature distribution for a two-dimensional plane extracted from three-dimensional interpolation of temperature sensor data during active desiccation. These data representations can be used to interpret the distribution of desiccation and when "significant" desiccation was obtained based on the distribution of evaporative cooling and post-cooling temperature increases. The progression of cooled zones shown at Days 14, 30, and 70 are indicators of desiccation activity (evaporative cooling) and the related dominant injected dry gas flow pattern. By Days 140 and 164, localized warming indicated that some zones had been desiccated. Desiccation, as indicated by cooler temperatures, continued to occur at other locations at these times. Interpretation of the two-dimensional temperature representations should consider that interpolation may not accurately reflect the temperature distribution away from the measurement point.

Comparative Assessment

The geophysical methods and temperature monitoring applied in the field test utilize substantially different methods to provide data for estimating the distribution and extent of moisture content changes during desiccation. For each method, there are benefits and limitations for use of these data to monitor desiccation based on the characteristics of the data collection, analysis techniques, and sources of error. These benefits and limitations also have implications for the application of desiccation treatment on a larger scale than was applied for the field test.

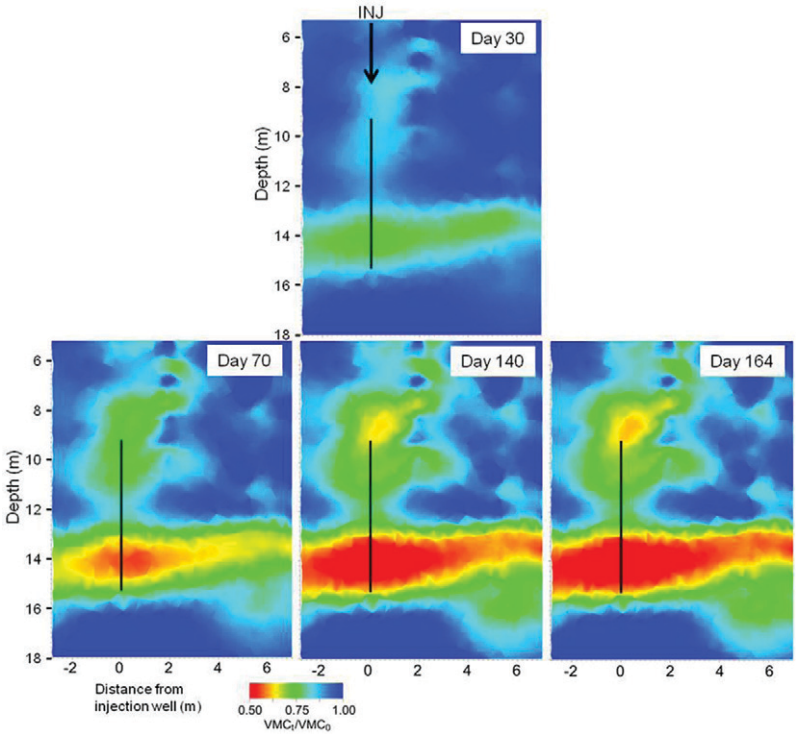

Fig. 12. Ratio of volumetric moisture content at time t (VMC_t) to predesiccation volumetric moisture content (VMC_0) with time along the axis between the injection (INJ) and extraction wells from cross-hole electrical resistivity tomography (ERT). The ERT data are from sensors at Locations S1 to S7 (Fig. 3). The black line indicates the screened section of the injection well.

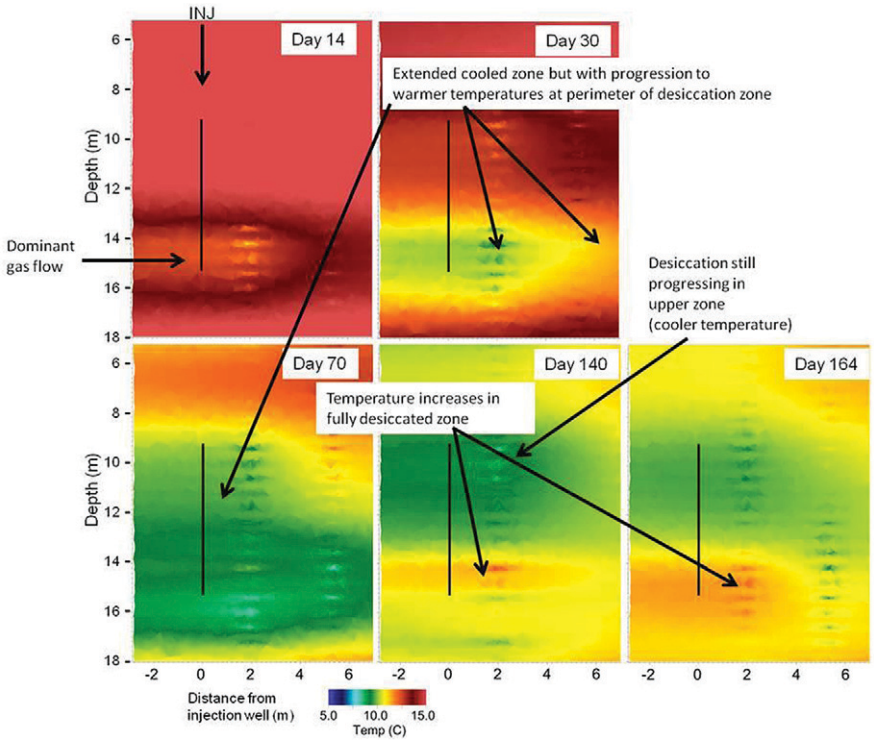

Fig. 13. Interpolated temperature response along the axis between the injection (INJ) and extraction wells, indirectly showing desiccation through the evaporative cooling effect. Temperatures drop while a zone is being desiccated. Once a zone is fully desiccated, there is no more evaporative cooling and the temperature rises toward the inlet temperature. Data are from sensors at Locations S1 to S7 (Fig. 3); the black line indicates the screened section of the injection well

Neutron moisture logging and GPR data can be converted using calibration approaches to provide VMC locally at a wellbore or within a two-dimensional plane, respectively. Electrical resistivity tomography cannot be directly converted to VMC, but changes in ERT-measured *C* can be converted to corresponding changes in VMC. Temperature monitoring cannot be related to VMC but is an indicator of desiccation based on evaporative cooling phenomena. Data sets also have different sources of error; examples here include the errors expected based on the low-loss assumption used for the GPR interpretation and the errors associated with the loss of electrode coupling on the ERT interpretation. Thus, each data set needs to be interpreted differently and carefully with respect to monitoring the distribution of desiccation and targeted threshold moisture content.

Neutron moisture logging of a borehole is a standard method for obtaining a high-resolution vertical profile (~7.5-cm vertical intervals) of the VMC that is accurate locally (~30-cm radius) with calibration to sediment data. Temporal resolution of the data depends on the manual survey frequency, which may lead to lower temporal resolution than for methods that can operate autonomously. Subsurface conditions would be expected to change most rapidly near a dry gas injection well, with responses becoming much slower at larger radial distances. Thus, the need for frequent data associated with reaching desiccation targets is related to the scale of the targeted treatment zone. For desiccation operational decisions, however, more frequent early-term data may be needed to help guide operational adjustments that may impact the overall long-term performance.

Interpolation of the VMC from neutron moisture logging data can be used to generate a three-dimensional image of moisture conditions that may be most appropriate for sites with significant anisotropy leading to dominantly horizontal soil gas flow. As the monitoring scale becomes larger, however, neutron data may become sparse compared with the targeted desiccation volume, depending on the number of access locations installed. For instance, if drying has occurred at one location but not yet at another location, interpolation cannot effectively project the extent of drying past the first location. As distances between monitoring locations grow larger, larger portions of the subsurface are essentially not monitored for a period of time by neutron data.

Cross-hole GPR provides the means to monitor VMC in two dimensions based on the propagation of energy through the subsurface between two logging boreholes. Thus, it provides data for interpretation of VMC distribution away from subsurface access points and does not require interpolation between access points like the neutron moisture logging data. Ground-penetrating radar provides high resolution within the survey plane due to the high vertical density of data from multiple offset surveys at the access locations. The GPR borehole spacing is constrained by energy propagation and generally needs to be <10 m for the vadose zone and even smaller for areas with high *C* (about 3 m at the desiccation test site). As with the neutron logging data, temporal resolution of the data depends on the manual survey frequency. High *C* at contaminated sites (e.g., due to high ionic contaminant concentrations in pore water such as are present in the lower portion of the test site) can severely impact the accuracy of the GPR estimate. When the ground has a high *C*, the low-loss assumption is not valid and the electromagnetic velocity is affected by both *C* and permittivity changes such that accurate conversion to VMC is difficult. In zones with significant desiccation, however, the *C* drops because the moisture content decreases. In those zones, the low-loss assumption may be valid and GPR data can be used to estimate the moisture content through Eq. [2] and [3]. At the field site, even very high initial *C* dropped to levels appropriate for the low-loss assumption in desiccated zones.

Cross-hole ERT provides the means to monitor the change in VMC in three dimensions based on the imaged *C* distribution in the subsurface between multiple electrodes. Decreases in temperature and moisture content occur during desiccation, both of which cause a decrease in *C*. Thus, to improve the accuracy of quantitative estimates of the moisture content change using ERT, a temperature correction is necessary. This correction is moisture content dependent, but in practice, a constant temperature correction factor is applied in the data inversion. In addition, increasing fluid conductivity with decreasing moisture content may dampen the ERT response and impact moisture content change estimates. Electrical resistivity tomography data provides limited resolution such that the distribution of spatial moisture content change is depicted with lower contrast than actually exists, appearing as a smoothed or blurred representation of actual changes. This issue is applicable with any geophysical method requiring an inversion, such as GPR; however, GPR generally provides higher spatial resolution than ERT given the same access points for electrodes and antennas. With ERT, spatial resolution can be adapted by modifying the electrode distribution and the proximity to the desiccation zone, and can be selected to be appropriate for the scale of the desiccation target and the resolution needed based on the monitoring goals. As shown in Fig. 6 and 12, ERT imaging resolution can change with time if electrodes have to be dropped from the network because of electrical coupling issues as the porous medium is desiccated. In the field test, maintaining electrical coupling was difficult in heavily desiccated zones, probably due to bentonite contraction and subsequent separation from electrodes. Full-scale applications would need to consider improved wetting capability or nonshrinkable grout around electrodes to maintain adequate coupling (e.g., neat Portland cement).

A significant benefit of the ERT method is that the data can be collected autonomously, which can greatly improve temporal resolution over manually collected data sets. Thus, ERT provides the potential for relatively automated imaging of desiccation progress. Electrical resistivity tomography derived changes in bulk conductivity provide qualitative information concerning when and where desiccation is occurring without interpretation. To be

quantitative, however, ERT images must be interpreted to relate the ERT-derived change in the VMC (e.g., VMC_t/VMC_0) at the available data resolution to the site-specific metrics for desiccation distribution and threshold moisture content targets. Potentially, using predesiccation measurements of the initial VMC, a threshold VMC change ratio for reducing the VMC to below a specified threshold could be set (e.g., if the target VMC is 0.02 and the initial VMC is about 0.06, a target change ratio would be about 0.3). Interpretation would need to consider that the ERT data represent average changes within the resolution control volume (e.g., for the field test, a volume of $\sim$1 m^3). Final VMC values may need to be confirmed at selected locations with another method like neutron logging or GPR. For the field test, with consideration of the ERT resolution issues at the bottom of the test zone, a VMC reduction of about 50% from the initial moisture content value corresponded to zones where other data also indicated significant desiccation.

Due to the evaporative cooling effect of desiccation, temperature data with time can also be used to interpret the desiccation distribution and roughly indicate achieving a threshold of significant desiccation based on the inflection of cooling to warming trends. Resolution for these determinations depends on sensor spacing, and interpolation of the data is required, with related issues as discussed for the neutron logging data. Temperature sensors are robust and relatively inexpensive, and data can be collected autonomously. Thus, temperature monitoring appears to be useful as part of a desiccation monitoring approach.

Conclusions

Monitoring the progression of in situ remedies such as desiccation is needed to provide information to guide operational decisions. Additionally, monitoring data are needed to determine when performance requirements, such as the size of the desiccated zone and the final moisture content, have been met. Monitoring options for in situ vadose zone remedies are limited, however, and implementation can be challenging due to subsurface properties and limited access. Geophysical monitoring methods were evaluated as part of a field-scale treatability test of desiccation at the Hanford site, with an emphasis on providing spatial and temporal information about the distribution of desiccation and the extent of moisture content reduction. The study also highlighted the benefits and limitations of different borehole and cross-hole methods for monitoring desiccation. Although the method evaluation objective of the study was met, future efforts using joint or coupled inversion approaches and more sophisticated petrophysical relationships (Ferré et al., 2009; Hubbard and Linde, 2011; Laloy et al., 2012) are expected to take advantage of the benefits and compensate for some of the method-specific limitations.

Traditional moisture content monitoring through neutron moisture logging is well established and provides detailed vertical profile information at discrete logging locations. Interpolation of multiple logging locations is possible but must be applied with caution because interpolation does not account for subsurface heterogeneities away from the logging locations and becomes less representative as the distance between logging locations increases. While GPR moisture content estimates are impacted by high C, estimates in low-C and significantly desiccated zones appear to be similar to neutron moisture data. Ground-penetrating radar scaling to larger applications may be limited by the need for relatively closely spaced logging access. Electrical resistivity tomography data can be collected autonomously for good temporal resolution and can provide estimates of moisture content change in three dimensions but not estimates of absolute moisture content; however, ERT implementation is readily scalable to larger sites. Interestingly, interpolation of temperature data, due to the evaporative cooling effect of desiccation, also provided useful three-dimensional information about the progress of desiccation and is a robust method for vadose zone implementation.

Acknowledgments

Primary funding for this research was provided by CH2M Hill Plateau Remediation Company, Richland, WA. Additional funding related to refinement of the data analysis techniques and conducting GPR surveys was provided by the USDOE Office of Groundwater and Soil Remediation and Richland Operations Office as part of the Deep Vadose Zone Applied Field Research Initiative. Pacific Northwest National Laboratory is operated by the Battelle Memorial Institute for the USDOE under Contract DE-AC06-76RLO 1830. Visualization software was provided by Lawrence Livermore National Laboratory using VisIt. Neutron moisture logging was conducted by the S.M. Stoller Corporation, Hanford Office, under contract to CH2M Hill Plateau Remediation Company, Richland, WA.

References

Archie, G.E. 1942. The electrical resistivity log as an aid in determining some reservoir characteristics. Trans. Am. Inst. Min. Metall. Pet. Eng. 146:54–62.

Annan, P. 2005. GPR methods for hydrogeological studies. In: Y. Rubin and S.S. Hubbard, editors, Hydrogeophysics. Water Sci. Technol. Lib. 50. Springer, Dordrecht, the Netherlands. p. 185–214.

Binley, A., G. Cassiani, R. Middleton, and P. Winship. 2002. Vadose zone model parameterisation using cross-borehole radar and resistivity imaging. J. Hydrol. 267:147–159. doi:10.1016/S0022-1694(02)00146-4

Binley, A., and A. Kemna. 2005. DC resistivity and induced polarization methods. In: Y. Rubin and S. Hubbard, editors, Hydrogeophysics. Water Sci. Technol. Lib. 50. Springer, Dordrecht, the Netherlands. p. 129–156.

Daily, W., and E. Owen. 1991. Cross-borehole resistivity tomography. Geophysics 56:1228–1235. doi:10.1190/1.1443142

Davis, J.L., and A.P. Annan. 1989. Ground-penetrating radar for high-resolution mapping of soil and rock stratigraphy. Geophys. Prospect. 37:531–551. doi:10.1111/j.1365-2478.1989.tb02221.x

Day-Lewis, F.D., J.M. Harris, and S.M. Gorelick. 2002. Time-lapse inversion of crosswell radar data. Geophysics 67:1740–1752. doi:10.1190/1.1527075

Dresel, P.E., D.M. Wellman, K.J. Cantrell, and M.J. Truex. 2011. Review: Technical and policy challenges in deep vadose zone remediation of metals and radionuclides. Environ. Sci. Technol. 45:4207–4216. doi:10.1021/es101211t

Ferré, T., L. Bentley, A. Binley, N. Linde, A. Kemna, K. Singha, et al. 2009. Critical steps for the continuing advancement of hydrogeophysics. Eos Trans. AGU 90:200. doi:10.1029/2009EO230004

Friedman, S.P. 2005. Soil properties influencing apparent electrical conductivity: A review. Comput. Electron. Agric. 46:47–50.

Greacen, E.L., R.L. Correll, R.B. Cunningham, O.C. Johns, and K.D. Nichols. 1981. Calibration. In: E.L. Greacen, editor, Soil water assessment by the neutron method. CSIRO, Melbourne, VIC, Australia, p. 50–78.

Grote, K., C. Anger, B. Kelly, S. Hubbard, and Y. Rubin. 2010. Characterization of soil water content variability and soil texture using GPR groundwave techniques. J. Environ. Eng. Geophys. 15:93–110. doi:10.2113/JEEG15.3.93

Hamamoto, S., P. Moldup, K. Kawamoto, and T. Komatsu. 2010. Excluded-volume expansion of Archie's law for gas and solute diffusivities and electrical and thermal conductivities in variably saturated porous media. Water Resour. Res. 46:W06514. doi:10.1029/2009WR008424

Han, M., S. Youssef, E. Rosenberg, M. Fleury, and P. Levitz. 2009. Deviation from Archie's law in partially saturated porous media: Wetting film versus disconnectedness of the conducting phase. Phys. Rev. E 79:031127. doi:10.1103/PhysRevE.79.031127

Hignett, C., and S.R. Evett. 2002. Neutron thermalization. In: J.H. Dane and G.C. Topp, editors, Methods of soil analysis. Part 4. Physical methods. SSSA Book Ser. 5. SSSA, Madison, WI. p. 501–521.

Hubbard, S.S., and N. Linde. 2011. Hydrogeophysics. In: P. Wilderer, editor-in-chief, Treatise on water science. Vol. 2. Academic Press, Oxford, UK. p. 401–434.

Hubbard, S.S., J.E. Peterson, E.L. Majer, P.T. Zawislanski, J. Roberts, K.H. Williams, and F. Wobber. 1997. Estimation of permeable pathways and water content using tomographic radar data. Leading Edge 16:1623–1628. doi:10.1190/1.1437539

Huisman, J.A., C. Sperl, W. Bouten, and J.M. Verstraten. 2001. Soil water content measurements at different scales: Accuracy of time domain reflectometry and ground-penetrating radar. J. Hydrol. 245:48–58. doi:10.1016/S0022-1694(01)00336-5

Jackson, M.J., and D.R. Tweeton. 1994. MIGRATOM: Geophysical tomography using wavefront migration and fuzzy constraints. Rep. Invest. 9497. U.S. Dep. of the Interior, Bureau of Mines, Washington, DC.

Johnson, T.C., R.J. Versteeg, A. Ward, F.D. Day-Lewis, and A. Revil. 2010. Improved hydrogeophysical characterization and monitoring through parallel modeling and inversion of time-domain resistivity and induced polarization data. Geophysics 75(4):WA27–WA41. doi:10.1190/1.3475513

Laloy, E., N. Linde, and J.A. Vrugt. 2012. Mass conservative three-dimensional water tracer distribution from Markov chain Monte Carlo inversion of time-lapse ground-penetrating radar data. Water Resour. Res. 48:W07510. doi:10.1029/2011WR011238

Ledieu, J., P. De Ridder, P. De Clerck, and S. Dautrebande. 1986. A method of measuring soil moisture by time-domain reflectometry. J. Hydrol. 88:319–328. doi:10.1016/0022-1694(86)90097-1

Lesmes, D., and S. Friedman. 2005. Electrical and hydrological properties. In: Y. Rubin and S. Hubbard, editors, Hydrogeophysics. Water Sci. Technol. Lib. 50. Springer, Dordrecht, the Netherlands. p. 87–128.

Oostrom, M., V.L. Freedman, T.W. Wietsma, and M.J. Truex. 2012a. Effects of porous medium heterogeneity on vadose zone desiccation: Intermediate-scale laboratory experiments and simulations. Vadose Zone J. 11(4). doi:10.2136/vzj2011.0168

Oostrom, M., T.W. Wietsma, J.H. Dane, M.J. Truex, and A.L. Ward. 2009. Desiccation of unsaturated porous media: Intermediate-scale experiments and numerical simulation. Vadose Zone J. 8:643–650. doi:10.2136/vzj2008.0182

Oostrom, M., T.W. Wietsma, C.E. Strickland, V.L. Freedman, and M.J. Truex. 2012b. Sensor and numerical simulator evaluation for porous medium desiccation and rewetting at the intermediate laboratory scale. Vadose Zone J. 11(1). doi:10.2136/vzj2011.0089

Or, D., and J.M. Wraith. 1999. Temperature effects on soil bulk dielectric permittivity measured by time domain reflectometry: A physical model. Water Resour. Res. 35:371–383. doi:10.1029/1998WR900008

Peterson, J.E., Jr. 2001. Pre-inversion corrections and analysis of radar tomographic data. J. Environ. Eng. Geophys. 6:1–18. doi:10.4133/JEEG6.1.1

Revil, M., M. Karaoulis, T. Johnson, and A. Kemna. 2012. Review: Some low-frequency electrical methods for subsurface characterization. Hydrogeol. J. 15:617–658. doi:10.1007/s10040-011-0819-x

Rubin, Y., and S. Hubbard, editors. 2005. Hydrogeophysics. Water Sci. Technol. Lib. 50. Springer, Dordrecht, the Netherlands.

Ma, R., A. McBratney, B. Whelan, B. Minasny, and M. Short. 2011. Comparing temperature correction models for soil electrical conductivity measurement. Precis. Agric. 12:55–66. doi:10.1007/s11119-009-9156-7

Serne, R.J., A.L. Ward, W. Um, B.N. Bjornstad, D.F. Rucker, D.C. Lanigan, and M.W. Benecke. 2009. Electrical resistivity correlation to vadose zone sediment and pore-water composition for the BC cribs and trenches area. PNNL-17821. Pac. Northw. Natl. Lab., Richland, WA.

Slater, L.D., and D.P. Lesmes. 2002. Electrical–hydraulic relationships observed for unconsolidated sediments. Water Resour. Res. 38:1213–1225. doi:10.1029/2001WR001075

Topp, G.C., J.L. Davis, and A.P. Annan. 1980. Electromagnetic determination of soil water content: Measurements in coaxial transmission lines. Water Resour. Res. 16:574–582. doi:10.1029/WR016i003p00574

Topp, G.C., and P.A. Ferré. 2002. Water content. In: J.H. Dane and G.C. Topp, editors, Methods of soil analysis. Part 4. Physical methods. SSSA Book Ser. 5. SSSA, Madison, WI. p. 417–545.

Topp, G.C., and W.D. Reynolds. 1998. Time domain reflectometry: A seminal technique for measuring mass and energy in soil. Soil Tillage Res. 47:125–132. doi:10.1016/S0167-1987(98)00083-X

Truex, M.J., M. Oostrom, V.L. Freedman, C.E. Strickland, and A.L. Ward. 2011. Laboratory and modeling evaluations in support of field testing for desiccation at the Hanford site. PNNL-20146. Pac. Northw. Natl. Lab., Richland, WA.

Truex, M.J., M. Oostrom, C.E. Strickland, G.B. Chronister, M.W. Benecke, and C.D. Johnson. 2012a. Field-scale assessment of desiccation implementation for deep vadose zone contaminants. Vadose Zone J. 11(4). doi:10.2136/vzj2011.0144

Truex, M.J., M. Oostrom, C.E. Strickland, T.C. Johnson, V.L. Freedman, C.D. Johnson, et al. 2012b. Deep vadose zone treatability test for the Hanford central plateau: Soil Desiccation Pilot Test results. PNNL-21369. Pac. Northw. Natl. Lab., Richland, WA.

Um, W., R.J. Serne, M.J. Truex, A.L. Ward, M.M. Valenta, C.F. Brown, et al. 2009. Characterization of sediments from the Soil Desiccation Pilot Test (SDPT) site in the BC cribs and trenches area. PNNL-18800. Pac. Northw. Natl. Lab., Richland, WA.

USDOE. 2008. Deep vadose zone treatability test plan for the Hanford central plateau. DOE/RL-2007-56. Rev. 0. USDOE Richland Operations Office, Richland, WA.

USDOE. 2010. Characterization of the Soil Desiccation Pilot Test site. DOE/RL-2009-119. Rev. 0. USDOE Richland Office, Richland, WA.

Van Overmeeren, R., S. Sariowan, and J. Geherls. 1997. Ground penetrating radar for determining volumetric soil water content: Results of comparative measurements at two test sites. J. Hydrol. 197:316–338. doi:10.1016/S0022-1694(96)03244-1

Vereecken, H., A. Binley, G. Gassiani, A. Revil, and K. Titov. 2006. Applied hydrogeophysics. NATO Sci. Ser., Earth Environ. Sci. 71. Springer, Dordrecht, the Netherlands.

Ward, A.L., M. Oostrom, and D.H. Bacon. 2008. Experimental and numerical investigations of soil desiccation for vadose zone remediation: Report for fiscal year 2007. PNNL-17274. Pac. Northw. Natl. Lab., Richland, WA.

Waxman, M.H., and L.J.M. Smits. 1968. Electrical conduction in oil-bearing sands. SPE J. 8:107–122.

Waxman, M.H., and E.C. Thomas. 1974. Electrical conductivities in shaly sands: I. The relation between hydrocarbon saturation and resistivity index; II. The temperature coefficient of electrical conductivity. J. Pet. Technol. 26:213–225.

White, I., and S.J. Zegelin. 1994. Electric and dielectric methods for monitoring soil-water content. In: L.G. Wilson et al., editors, Handbook of vadose zone characterization and monitoring. CRC Press, Boca Raton, FL.